Optics Communications 282 (2009) 4292–4295

Contents lists available at ScienceDirect

Optics Communications

journal homepage: www.elsevier.com/locate/optcom

Properties of defect modes in one-dimensional photonic crystals containing two nonlinear defects

Xia Li [a,b,*], Kang Xie [a], Hai-Ming Jiang [a]

[a] School of Opto-electronic Information, University of Electronic Science and Technology of China, Chengdu 610054, China
[b] Department of Physics, Chengdu University of Technology, Chengdu 610059, China

ARTICLE INFO

Article history:
Received 9 April 2009
Received in revised form 24 July 2009
Accepted 24 July 2009

Keywords:
Photonic crystal
Defect mode
Optical bistability
Defect coupling

ABSTRACT

Transmission properties of one-dimensional photonic crystal with two nonlinear defects were investigated based on the nonlinear transfer matrix method. From the inspection of the optical bistabilities around different defect modes, it was found that the threshold of bistability for the bonding mode is always lower than that for the anti-bonding mode. When intensity of the incident wave increases bistability could happen at any wavelength larger than the resonance wavelength of the linear anti-bonding mode in the gap. The threshold of bistability increases initially with the wavelength, then decreases sharply in reaching the resonance wavelength of the linear bonding mode. The coupling behavior of the two defects was also discussed, and it was found that the threshold of bistability increases with the distance between the two defects. A flat spectrum similar to that formed in the photonic crystal molecules was obtained under certain incident intensity.

1. Introduction

Photonic crystals with single defect are interesting because of their potential application in the fabrication of lasers [1], light-emitting diodes [2], and filters [3]. Recently, the structure with coupled defects has attracted much more attention. Such structure has some important functions which cannot be achieved by single defect. For example, it can realize the function of coupled cavity waveguides [4,5], waveguide bends and splitters [6]. Many works have been focused on analyzing the coupling behavior of defects and finding the impurity bands [7,8]. In a one-dimensional photonic crystals (1D PC) molecular structure with two linear defects, the spectra are composed of clear bonding and anti-bonding states when the transmission phase of PC atoms is close to zero, while the spectra are flat on top when the transmission phase of PC atoms is close to 90° [9,10]. The coupled cavity waveguides (CCW) composed of the PC molecular with flat spectra could have quasi-flat impurity bands suitable for the transmission of ultrashort pulses [11]. When nonlinear defects are periodically introduced into the CCW there would be a dynamical band gap appearing at the center of the impurity band. This gap could be used as a very efficient switching mechanism for ultrashort pulses.

On the other hand, some works put more attention on the properties of defect modes. In the one-dimensional PC with two linear defects [12], the spectrum separation of the two defect modes are related to the physical distance between the two defects and the refractive index of the defects. When one of the two defects is a layer of dispersive medium and the other is a layer of nonlinear medium [13], the threshold intensity is much lower than that of a structure without the dispersive layer.

In this paper the transmission properties of one-dimensional PC with two coupled nonlinear defects were investigated based on the nonlinear transfer matrix method (NTMM) [14]. The threshold of bistability at different defect modes induced by different incident intensity was analyzed, and the difference between the anti-bonding mode and the bonding mode under the same incident intensity was investigated. The coupling behavior of the two nonlinear defects in different symmetric structures was discussed, and finally a flat spectrum similar to that of a PC molecular under certain incident intensity was obtained and analyzed.

2. PC structure and the nonlinear transfer matrix method

The structure discussed in this work is shown in Fig. 1. This photonic crystal is composed of materials A and B stacked alternately along the z axis, with the refractive indexes $n_a = 2.5$, $n_b = 2.0$. The thickness $d_a = 2\lambda_0/n_a$, $d_b = 2\lambda_0/n_b$, where $\lambda_0 = 450$ nm is a reference wavelength. The two nonlinear layers D are the defects of the structure, with refractive index $n_d^2 = n_0^2 + \chi^{(3)}I$ and thickness $d_d = 2d_a$. Here $\chi^{(3)}$ is the small positive, third-order susceptibility coefficient accounting for the nonlinear interactions in the structure and I is the field intensity.

* Corresponding author. Address: Department of Physics, Chengdu University of Technology, Chengdu 610059, China.
E-mail address: lixiamail@tom.com (X. Li).

0030-4018/$ - see front matter © 2009 Elsevier B.V. All rights reserved.
doi:10.1016/j.optcom.2009.07.061

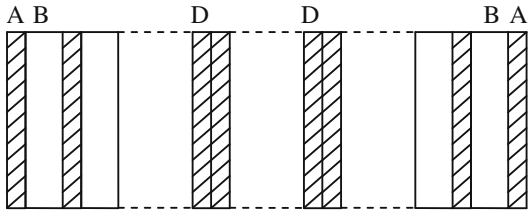

Fig. 1. Sketch of the one-dimensional PC structure with two nonlinear defects.

The amplitude of electric-field E_j inside the jth layer can be written as

$$E_j = E_{Fj}\exp[-ik_jz + i\varphi_{Fj}(z)] + E_{Bj}\exp[ik_jz + i\varphi_{Bj}(z)]$$

where E_{Fj} and E_{Bj} is respectively the amplitude of the forward and backward propagating wave in the jth layer, φ_{Fj} and φ_{Bj} are the nonlinearly induced phase changes. The amplitudes of the jth layer are related to the amplitudes of the layer $j+1$ by a matrix $M_{j,j+1}$

$$\begin{pmatrix} E_{Fj} \\ E_{Bj} \end{pmatrix} = M_{j,j+1}\begin{pmatrix} E_{Fj+1} \\ E_{Bj+1} \end{pmatrix}$$

The elements of the matrix are

$$m_{11} = \frac{(k_j+k_{j+1})}{2k_j}e^{2ik_jL_j}, \quad m_{12} = \frac{(k_j-k_{j+1})}{2k_j}e^{2i(k_j+k_{j+1})L_i}$$
$$m_{21} = \frac{(k_j-k_{j+1})}{2k_j}e^{-i[\varphi_{Bj}(L_j)-\varphi_{Fj}(L_j)]}, \quad m_{22} = \frac{(k_j+k_{j+1})}{2k_j}e^{2ik_{j+1}L_j-i[\varphi_{Bj}(L_j)-\varphi_{Fj}(L_j)]}$$

where L_j is the ending z coordinate of the jth layer, k_j is the wave number in the jth layer. The nonlinear phase shift in the jth layer is

$$\Delta\varphi_j = \varphi_{Bj}(L_j) - \varphi_{Fj}(L_j) = \frac{6\pi\chi_j^{(3)}(|E_{Fj}|^2 + |E_{Bj}|^2)d_d}{\varepsilon_0 n_{0j}^2 c\lambda}$$

where $\chi_j^{(3)}$ is the third-order susceptibility, describing the Kerr effect of the jth layer, n_{0j} is the linear index of refraction, and λ is the free space wavelength of the incident wave. Since the layer $n+1$ extends to infinity, there is no backward propagating wave in this layer. By working backward, we can calculate the amplitude in the nth layer and other preceding layers from the outgoing wave E_T so the incident wave is related to the transmitted wave by

$$\begin{pmatrix} E_I \\ E_R \end{pmatrix} = M\begin{pmatrix} E_T \\ 0 \end{pmatrix}$$

where $M = M_{0,1}\cdots M_{j,j+1}\cdots M_{n,n+1}$. The transmission coefficient is obtained as: $t = \frac{|E_T|^2}{|E_I|^2} = \frac{1}{|M(1,1)|^2}$.

3. Optical bistability around the defect modes

The transmission properties of the structure for linear defects ($\chi^{(3)} = 0$) are shown in Fig. 2. It is seen that for different positions of defect layers (the distance between the two defects remains unchanged), the defect modes resonate at the same wavelengths but with different transmission coefficients. The transmission coefficients of the two defect modes in the symmetric structure $(AB)_6DB(AB)_2D(BA)_6$ are close to 1. On the other hand they are lower in the asymmetric structure $(AB)_4DB(AB)_2D(BA)_8$ and $(AB)_7DB(AB)_2D(BA)_5$. So the symmetric structure $(AB)_6DB(AB)_2D(BA)_6$ was chosen for the subsequent analysis.

The transmission peaks around $\lambda = 398.3$ nm and $\lambda = 401.7$ nm shown in Fig. 2 indicate the onset of defect modes. The transmitted intensities of the symmetric structure $(AB)_6DB(AB)_2D(BA)_6$ at $\lambda = 399.3$ nm and $\lambda = 402.4$ nm are plotted against the incident intensity in Figs. 3a, b and c for $\chi^{(3)} \neq 0$. The reduced intensity used in this plot is defined as $I_{\text{red}} = n_j^{(2)}I$, where $n_j^{(2)} = \frac{\chi_j^{(3)}}{\varepsilon_0 n_{0j}^2 c}$. Bistable

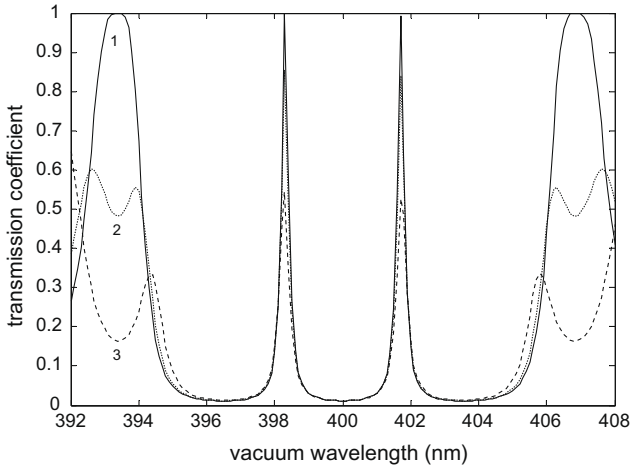

Fig. 2. The different spectra for the three different structures. Curve 1: $(AB)_6D$-$B(AB)_2D(BA)_6$; curve 2: $(AB)_7DB(AB)_2D(BA)_5$; curve 3: $(AB)_4DB(AB)_2D(BA)_8$.

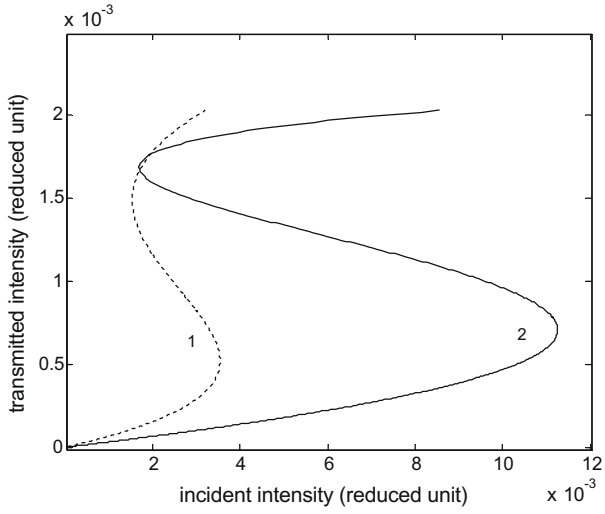

Fig. 3a. Transmitted intensity versus incident intensity at $\lambda = 402.4$ nm (curve 1) and $\lambda = 399.3$ nm (curve 2).

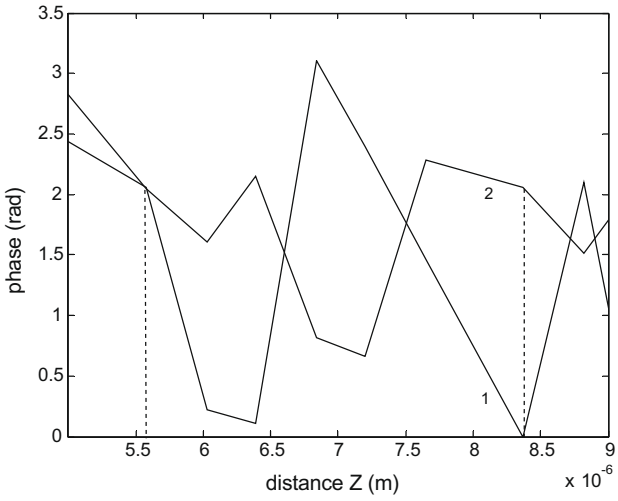

Fig. 3b. Phase profiles of the defect modes: curve 1 $\lambda = 399.3$ nm; curve 2 $\lambda = 402.4$ nm. The locations of the two defects are indicated by the two vertical lines.

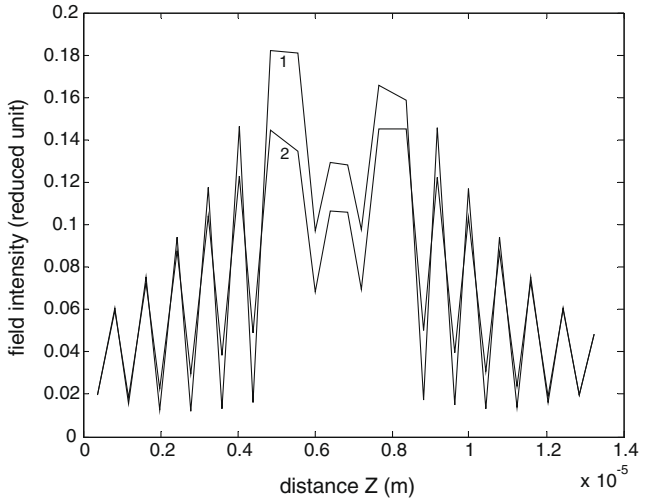

Fig. 3c. Intensity profiles of the two defect modes: curve 1 $\lambda = 402.4$ nm; curve 2 $\lambda = 399.3$ nm.

responses are clearly evident. It is seen from Fig. 3a that the threshold of bistability is larger for the defect mode at shorter wavelength, while it is smaller for the defect mode at longer wavelength. The reason lies in the fact that the defect mode resonates at longer wavelength is a "bonding" mode while the defect mode resonates at the shorter wavelength is an "anti-bonding" mode [15,16]. It is seen from Fig. 3c that for the same incident intensity, the peaks of the bonding mode that appear around the nonlinear defects are higher than those of the anti-bonding mode. To achieve the same level of nonlinear Kerr effect to trigger the bistability, larger incident intensity is needed for the anti-bonding mode than that for the bonding mode. This leads to a higher threshold of bistability for the anti-bonding mode than that for the bonding mode.

For the "bonding" mode the fields oscillating at the two defects are nearly in phase while for the "anti-bonding" mode the fields oscillating at the two defects are nearly $\pi/2$ out of phase. The phase profiles of the linear bonding mode and the linear anti-bonding mode in the structure are shown in Fig. 3b. For this example, the electric-fields at the two defects have a phase difference of 0.011 rad $\approx 0.62°$ for the bonding mode. For the anti-bonding mode on the other hand, the phase difference is 2.044 rad $\approx 117°$. The different phase differences enable such modes excitable individually by signals with different matching symmetries. Although the curves of phase profiles are different for the two defect modes, their intensity profiles seem to resemble each other closely. The "bonding" mode and the "anti-bonding" mode have nearly identical field distributions in the PC. They only differ slightly around the defects and the coupling region as shown in Fig. 3c.

In fact, bistable response was found to occur for incident wave of wavelength from 398.6 to 405 nm for $\chi_3 > 0$. Because of that, the wavelength of defect modes increase from $\lambda = 398.6$ nm with the increase of incident intensity. It was also found that the threshold of bistability increases sharply around $\lambda = 398.6$ nm and decreases sharply just before $\lambda = 402$ nm. From $\lambda = 402$ nm to $\lambda = 405$ nm the threshold of bistability increases monotonously with wavelength. This characteristic is evident in Fig. 4.

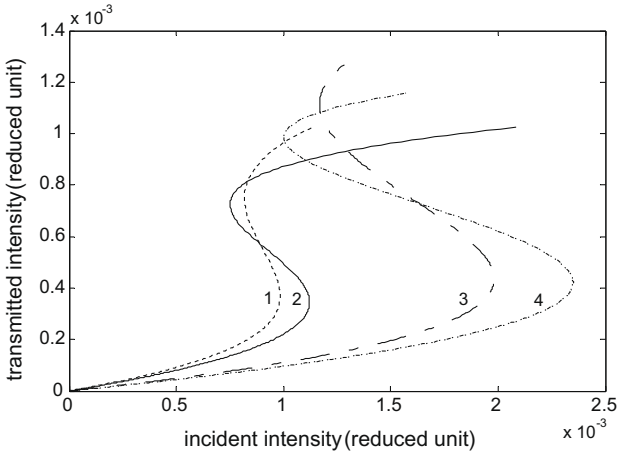

Fig. 4. Transmission curves at different wavelengths in the gap. Curve 1: $\lambda = 402$ nm; curve 2: $\lambda = 398.6$ nm; curve 3: $\lambda = 402.1$ nm; curve 4: $\lambda = 398.7$ nm.

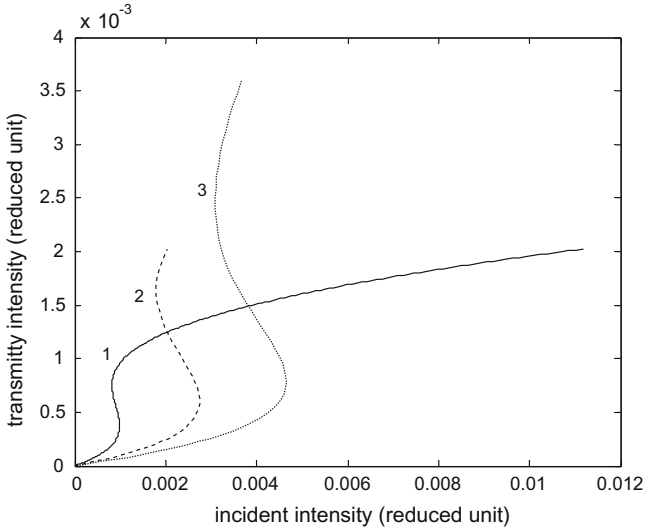

Fig. 5a. Transmission curves around the resonant wavelength of the bonding mode in different symmetric structures. Curve 1: $(AB)_6DB(AB)_2D(BA)_6$ at $\lambda = 402$ nm; curve 2: $(AB)_5DB(AB)_4D(BA)_5$ at $\lambda = 401.5$ nm; curve 3: $(AB)_4DB(AB)_6D(BA)_4$ at $\lambda = 401.3$ nm.

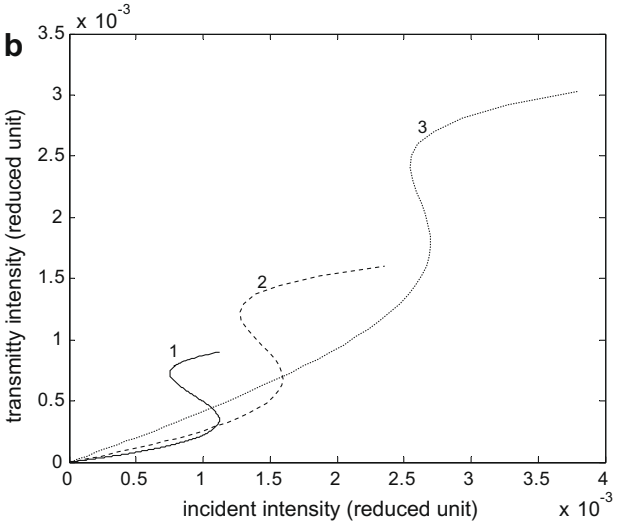

Fig. 5b. Transmission curves around the resonant wavelength of the anti-bonding mode in different symmetric structures. Curve 1: $(AB)_6DB(AB)_2D(BA)_6$ at $\lambda = 398.6$ nm; curve 2: $(AB)_5DB(AB)_4D(BA)_5$ at $\lambda = 399.3$ nm; curve 3: $(AB)_4DB(AB)_6D(BA)_4$ at $\lambda = 399.8$ nm.

4. Coupling between the pair of defect modes

The coupling of two linear defects has been intensively studied in the literature. In this work the concern is on the coupling of two nonlinear defects. Discussion is concentrated on the coupling phenomenon associated with nonlinearity such as optical bistability.

The bistabilities in three symmetric structures with different defect locations were studied. The coupling strength between two linear defects decreases as their distance increases [12]. From the inspection of Figs. 5a and b, it was found that both the bonding mode and the anti-bonding mode occur at different wavelength for different structure (really different distance between defects). It was also found that the thresholds of bistability for both modes increase when the two defects move further apart. This result is consistent with that of the linear coupling. The dielectric multilayer plays the role of scattering potential barrier separating the two defects that play the role of cavities. As the thickness of the barrier increases, the tail of one cavity mode has to span a larger gap to reach the other cavity. Therefore stronger incident intensity is needed to generate the same level of Kerr effect in the medium for the completion of bistable transition, when the distance between the two defects is enlarged.

A comparison of thresholds for bistability between a cavity with one defect and a cavity with two defects is presented in Fig. 6 for incident waves of the same wavelength. It can be seen that as the gap between the two defects increases, the threshold for bistability increases. In the limit of infinite gap, the value of threshold for bistability for a cavity with two defects approaches the value of threshold for bistability for a cavity with one defect.

A flat spectrum similar to that formed in PC molecular was discovered by varying the incident intensity in the structure $(AB)_7DBD(BA)_7$. The corresponding transmission characteristic is shown in Fig. 7. This interesting flat spectrum appears around an incident intensity of $I_i = 0.0722$ in the reduced units. It was formed by a mechanism different from that of the PC molecular. This nonlinear phenomenon could find applications in switchable band pass filters.

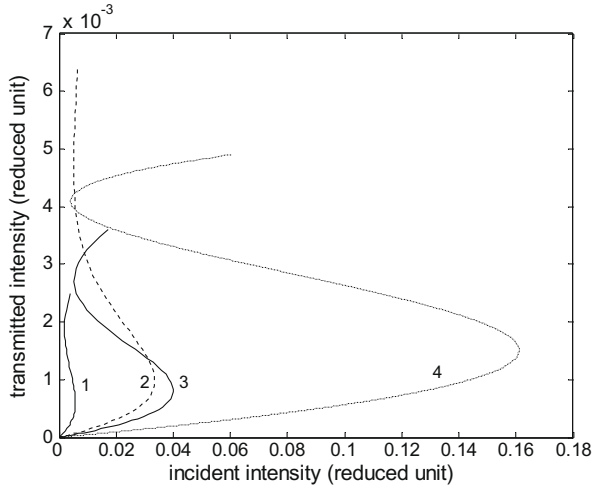

Fig. 6. Transmission curves at $\lambda = 402.3$ nm for a cavity with one defect and for a cavity with two defects separated by gaps of different thicknesses. Curve 1: $(AB)_6DB(AB)_2D(BA)_6$; curve 2: $(AB)_5DB(AB)_4D(BA)_5$; curve 3: $(AB)_4DB(AB)_6D(BA)_4$; curve 4: $(AB)_7D_2(BA)_7$.

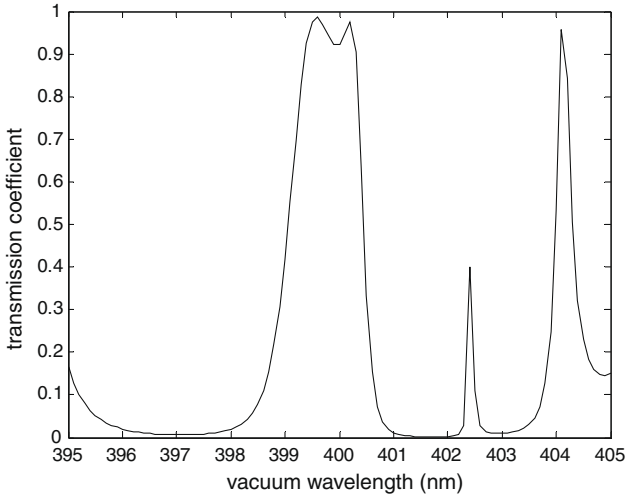

Fig. 7. Flat spectrum in the structure $(AB)_7DBD(BA)_7$ at incident intensity $I_i = 0.0722$ (reduced units).

5. Conclusion

The properties of defect modes in one-dimensional PC with two nonlinear defects were studied. The symmetric structure has maximum transmission coefficient in the linear limit so this structure was chosen for the analysis of nonlinear defect modes. Bistable responses near both the bonding mode and the anti-bonding mode were observed. Because of the primary difference between the bonding mode and the anti-bonding mode, the thresholds of bistability are different at the resonant wavelengths of the two defect modes. The threshold of bistability increases with wavelength near the resonant wavelength of the linear anti-bonding mode, while it decreases with wavelength near the resonant wavelength of the linear bonding mode. The coupling behavior of the two defects was discussed in connection with the onset of bistability. Finally an interesting flat spectrum similar to that formed in the PC molecular was found and the condition of its occurrence was identified.

Acknowledgement

This work was supported by NSFC (Project Numbers 60607005 and 60588502).

References

[1] W.D. Zhou, J. Sabarinathan, P. Bhattacharya, B. Kochman, E.W. Berg, P.C. Yu, S.W. Pang, IEEE J. Quantum Electron. 37 (2001) 1153.
[2] Michael W. Feise, Ilya V. Shadrivov, Yuri S. Kivshar, Phys. Rev. E 71 (2005) 037602.
[3] Bong-Shik Song, Takashi Asano, Yoshihiro Akahane, Yoshinori Tanaka, Susumu Noda, Member, IEEE J. Lightwave Technol. 23 (2005) 1449.
[4] Mehmet Bayindir, B. Temelkuran, E. Ozbay, Phys. Rev. B 61 (2000-II) R11855.
[5] Y.J. Chai, C.N. Morgan, R.V. Penty, I.H. White, T.J. Karle, T.F. Krauss, IEE Proc. Optoelectron. 151 (2004) 109.
[6] Mehmet Bayindir, B. Temelkuran, E. Ozbay, Appl. Phys. Lett. 77 (2000) 3902.
[7] Sheng Lana, Hiroshi Ishikawa, J. Appl. Phys. 91 (2002) 2573.
[8] Sheng Lana, Yoshimasa Sugimotoa, Satoshi Nishikawab, Naoki Ikedaa, Tao Yanga, Kozyo Kanamotoa, Hiroshi Ishikawaa, Kiyoshi Asakawaa, Proc. SPIE 4870 (2002) 368.
[9] Sheng Lan, Satoshi Nishikawa, Yoshimasa Sugimoto, Naoki Ikeda, Kiyoshi Asakawa, Hiroshi Ishikawa, Phys. Rev. B 65 (2002) 165208.
[10] Xu-sheng Lin, Xiong-wen Chen, Shen Lan, Chin. Phys. Lett. 22 (2005) 1698.
[11] M. Maksimovic, M. Hammer, E. van Groesen, Proc. SPIE 6896 (2008) 689603.
[12] Ji-guo Gen, Zong-hua Shi, Ke-zhu Yan, J. Optoelectron. Laser 17 (2006) 1497.
[13] Qing-hua Liao, Nian-hua Liu, Phys. D 210 (2005) 241.
[14] Jan Danckaert, Kristel Fobelets, Irina Veretennicoff, Phys. Rev. B 44 (1991) 8214.
[15] S.V. Zhukovsky, D.N. Chigrin, A.V. Lavrinenko, J. Kroha, Proc. SPIE 6725 (2007) 67250R.
[16] Irina V. Kabakova, Bill Corcoran, Jeremy A. Bolger, Martijn de Sterke, Benjamin J. Eggleton, Opt. Exp. 17 (2009) 5083.